Journal of Biomedical Optics 7(4), 618–627 (October 2002)

Imaging caries lesions and lesion progression with polarization sensitive optical coherence tomography

Daniel Fried
John Xie
University of California, San Francisco
Department of Preventive and Restorative Dental Science
San Francisco, California 94143

Sahar Shafi
California State University, Fresno
Fresno, California 93740

John D. B. Featherstone
Thomas M. Breunig
Charles Le
University of California, San Francisco
Department of Preventive and Restorative Dental Science
San Francisco, California 94143

Abstract. New diagnostic tools are needed for the characterization of dental caries in the early stages of development. If carious lesions are detected early enough, they can be arrested without the need for surgical intervention. The objective of this study was to demonstrate that polarization sensitive optical coherence tomography (PS-OCT) can be used for the imaging of early caries lesions and for the monitoring of lesion progression over time. High-resolution polarization resolved images were acquired of natural caries lesions and simulated caries lesions of varying severity created over time periods of 1 to 14 days. Linearly polarized light was incident on the tooth samples and the reflected intensity in both orthogonal polarizations was measured. PS-OCT was invaluable for removing the confounding influence of surface reflections and native birefringence necessary for the enhanced resolution of the surface structure of caries lesions. This study demonstrated that PS-OCT is well suited for the imaging of interproximal and occlusal caries, early root caries, and for imaging decay under composite fillings. Longitudinal measurements of the reflected light intensity in the orthogonal polarization state from the area of simulated caries lesions linearly correlated with the square root of time of demineralization indicating that PS-OCT is well suited for monitoring changes in enamel mineralization over time. [DOI: 10.1117/1.1509752]

Keywords: polarization sensitive optical coherence tomography; dental caries; demineralization; enamel and dentin; near-IR imaging.

Paper JBO 02005 received Jan. 16, 2002; revised manuscript received Apr. 9, 2002; accepted for publication May 8, 2002.

1 Introduction

New, more sophisticated diagnostic tools are needed for the detection and characterization of caries lesions in the early stages of development. If carious lesions are detected early enough, they can be arrested/reversed by nonsurgical means through fluoride therapy, anti-bacterial therapy, dietary changes, or by low intensity laser irradiation.[1] Furthermore, clinicians need an imaging technology employing nonionizing radiation to aid in caries management and diagnosis, to reliably track the course of caries lesions over an extended time period in order to determine whether the lesion is active and expanding, requiring intervention or whether the lesion has been arrested. Such technology would also enable nondestructive *in vivo* monitoring for short term clinical trials of anti-caries agents such as fluoride containing dentifrices. During the past century the nature of dental decay or dental caries in the U.S. has changed markedly due to the introduction of fluoride to the drinking water, the advent of fluoride dentifrices and rinses, and improved dental hygiene. In spite of these advances, dental decay continues to be the leading cause of tooth loss in the U.S.[2–4] The nature of the caries problem has changed dramatically with the majority of newly discovered caries lesions being highly localized to the occlusal pits and fissures of the posterior dentition and the interproximal contact sites between teeth. These early carious lesions are often obscured or ''hidden'' in the complex and convoluted topography of the pits and fissures or are concealed by debris that frequently accumulates in those regions of the posterior teeth. Moreover, such lesions are difficult to detect in the early stages of development. Caries lesions are usually not detected until after the lesions have progressed to the point at which surgical intervention and restoration are necessary, often resulting in the loss of healthy tissue structure and weakening of the tooth. Carious lesions also occur adjacent to existing restorations and diagnostic tools are needed to diagnose the severity of those lesions and determine if an existing restoration needs to be replaced. The diagnostic and treatment paradigms that were developed in the past such as radiography are adequate for large, cavitated lesions, however they do not have sufficient sensitivity or specificity for the diagnosis of early noncavitating caries, root surface caries, or secondary caries.

The optical properties of tooth enamel and dentin change markedly as a result of demineralization during the caries process, therefore caries detection schemes that exploit such changes hold considerable promise for the early detection and characterization of caries lesions.[5–9] The principal factor limiting optical transmission through the tooth in the visible range from 400 to 700 nm is light scattering in sound enamel and dentin.[10,11] The magnitude of light scattering in dental

Address all correspondence to Daniel Fried. Tel. 415-502-6641; Fax: 415-502-6642; E-mail: dfried@itsa.ucsf.edu

1083-3668/2002/$15.00 © 2002 SPIE

enamel decreases as $(1/\lambda^3)$, where λ is the wavelength, due to the size of the principal scatterers in enamel.[11] Therefore, we hypothesize that the near-IR region from 830 to 1550 nm offers the greatest potential for new optical imaging modalities due to the weak scattering and absorption in sound dental hard tissue.[12] At longer wavelengths, absorption of light by the water in the tissue increases markedly reducing the penetration of IR light.

Two optical diagnostic systems for caries detection have recently received FDA approval. A digital fiber optic transillumination system, called DiFoti, that utilizes white light for the detection of caries lesions, has been developed by Electro-optics Sciences, Irvington, NY.[13] This device is suitable for inter-proximal lesions, however, the usefulness for occlusal lesions has not yet been established.

Bacteria produce significant amounts of porphyrins and dental plaque fluoresces upon excitation with red light.[14] A caries detection system, the Diagnodent™ (Kavo, Germany), was recently developed and received FDA approval in the U.S. This device uses a diode laser and a fiber optic probe designed to detect the near-IR fluorescence from porphyrins. Although this must be considered a major step towards better caries detection in occlusal surfaces, it detects lesions in the later stage of development after the caries lesions have penetrated into the dentin and accumulated a considerable amount of bacteria. Moreover, the Diagnodent has a poor sensitivity ($\sim$40%) for lesions confined to enamel[15] and it does not provide information about the lesion depth and the degree of severity.[16,17]

Hafstroem-Bjoerkman et al.[18] established an experimental relationship between the loss of fluorescence intensity, presumably from the underlying dentin, and the extent of enamel demineralization.[18] The method was subsequently labeled the QLF method, for quantitative laser fluorescence. An empirical relationship between overall lesion demineralization (ΔZ) versus loss of fluorescence, was established which can be used to monitor lesion progression on smooth surfaces.[19–21] Unfortunately, QLF cannot readily be applied to occlusal and interproximal lesions that constitute the majority of carious lesions. Furthermore, this fluorescence method does not provide information about the subsurface characteristics of the lesion.

Optical coherence tomography (OCT) is a noninvasive technique for creating cross-sectional images of internal biological structure.[22] The intensity of backscattered light is measured as a function of its axial position (depth) in the tissue. Low coherence interferometry is used to acquire the intensity of backscattered light and reflected as a function of position within the tissue with a resolution of $\sim$20–30 μm. Lateral scanning of the probe beam across the tooth is then used to generate a two-dimensional intensity plot, similar to ultrasound images, called a ''b scan.'' The one-dimensional analog of OCT, optical coherence domain reflectometry (OCDR) was first developed as a high-resolution ranging technique for characterization of optical components.[23,24] Huang et al.[25] combined transverse scanning with a fiber optic OCDR system to produce the first OCT cross-sectional images of biological microstructure. The first images of the soft and hard tissue structures of the oral cavity were acquired by Colston et al.[26–28] Baumgartner et al.[29–31] presented the first polarization resolved images of dental caries, however the penetration depth was limited and the image quality was poor due to the limited source intensity. Feldchtein et al.[32] presented high-resolution dual wavelength 830 and 1280 nm images of dental hard tissues, enamel and dentin caries and restorations *in vivo*. Wang et al.[33] measured the birefringence in dentin and enamel and suggested that the enamel rods act as waveguides. The following year, Everett et al.[34] presented polarization resolved images using a high power 1310 nm broadband source and a bulk optic polarization sensitive optical coherence tomographic imaging (PS-OCT) system. In those images changes in the mineral density of tooth enamel were resolvable to depths of 2–3 mm into the tooth. Otis et al.[35] have demonstrated the improved imaging characteristics of a system operating at 1310 vs 850 nm.

According to Kidd,[36] 75% of operative dentistry is the replacement of existing restorations and secondary caries is the most common reason given for replacing both amalgam and composite fillings. PS-OCT is well suited for the detection of secondary caries since restorative materials have markedly different scattering properties compared to dental hard tissues. Colston[28] and Feldchtein[32] have shown that OCT can be used to differentiate between restorative materials and enamel and detect decay around the periphery of a restoration.[32]

Root caries is an increasing problem among our aging population and is the principal reason for tooth loss over the age of 44.[37] The scattering coefficient of dentin is much higher than enamel, therefore the penetration depth is more limited than for enamel.[10,11,38] However, early root caries is localized on the surface of the dentin and cementum and can be easily imaged using OCT.[32]

In this paper, we present images of occlusal and interproximal lesions, early root caries lesions and simulated caries lesions beneath composite fillings acquired using an all polarization maintaining (pm)-fiber PS-OCT system operating at 1310 nm. We also demonstrate that PS-OCT can be used effectively to monitor the longitudinal progression of simulated caries lesions using three dissolution models.

2 Materials and Methods

2.1 Sample Preparation

Sound and carious human permanent molars or premolars collected from oral surgeons in the San Francisco area and bovine incisors, obtained from a slaughterhouse and sterilized using gamma sterilization, were used for these studies. Three different types of tooth samples were prepared for imaging.

Polished Bovine Tooth Sections (5×5×2 mm³)

Sections $5\times5\times2$ mm^3 with an intact layer of enamel 1–2 mm thick were fabricated from sound bovine incisors to be used for the initial test samples (Sec. 3.1) and the demineralization studies of Sec. 3.4. The outer layer of cementum was removed from each incisor and the surface was cut to produce a flat surface. The surface was serial polished to produce a 1 μm surface finish using 600 grit silicon carbide abrasive followed by 6, 3, 1 μm diamond suspensions.

Sound Human Tooth Sections (4×4×2 mm³)

In addition, $4\times4\times2$ mm^3 sections were cut from the crowns of extracted, sound human third molars for longitudinal studies of lesion progression (Sec. 3.4). Human sections were polished with 600 grit silicon carbide abrasive paper to remove approximately 20–50 μm of the outer enamel. This procedure produces an enamel surface that has been shown to allow the formation of uniform and consistent caries-like lesions in our *in vitro* models.[39] A consistent ''model'' surface is important in order to reduce large variations during artificial lesion formation.[39] The human sections were not cut to be flat or highly polished using the diamond suspensions as was done for the bovine sections.

Whole Teeth with Carious Lesions

Whole tooth samples containing suspected occlusal and interproximal (white-spot) lesions (Secs. 3.2 and 3.3) were selected by visual examination for imaging by PS-OCT. Teeth were brushed with a 1% detergent solution and rinsed with doubly de-ionized water. The surface of the teeth showing natural caries lesions was not polished or modified in any way before images were acquired. A total of 20 extracted teeth were examined using PS-OCT and the images of Figures 4 and 5 contain one representative image of each lesion type.

Simulated-Caries Lesions

Lesions were produced in both the prepared human and bovine tooth sections described above using well-characterized demineralizing and remineralizing solutions[39–41] for varying time periods to produce simulated caries lesions of varying severity. Three simulated caries methods were used that produced different lesion morphology and varied in the rate of demineralization. During exposure of the sections to the demineralizing and remineralizing solutions half of each section was covered with an acid resistant varnish to protect the underlying surface to leave an area of sound enamel for comparison (see Figure 2).

In the first method, the straight demineralization model, each bovine section ($5\times5\times2$ mm^3) was immersed in 40 mL aliquots of a buffer solution containing 2.0 mmol/L calcium, 2.0 mmol/L phosphate and 0.075 mol/L acetate maintained at *p*H 4.3 and a temperature 37 °C for periods of 14, 24, 48, 96, and 192 h. A total of ten sections were used with two sections for each time period. This model results in rapid erosion of the enamel surface and does not accurately represent the ''acid challenge'' experienced in the mouth that consists of cycles of demineralization followed by remineralization as the *p*H changes before and after meals.

The second model, the *p*H cycling model, replicates this cycle of demineralization and remineralization that takes place naturally in the mouth as the *p*H fluctuates before and after meals.[39–41] Human tooth sections ($4\times4\times2$ mm^3) were exposed for 1, 3, 6, 9, and 14 days to a daily regimen of 6 h demineralization followed by 17 h remineralization. A total of 25 sections were used with five sections for each time period. In this model a surface zone is created due to remineralization and erosion of the surface does not occur as the lesion progresses in depth. For *p*H cycling each block was exposed to the demineralizing solution used in the first model described above for 6 h each day of the treatment at a *p*H of 4.5 followed by immersion overnight for 17 h in a remineralizing solution of 1.5 mmol/L calcium, 0.9 mmol/L phosphate, 150 mmol/L KCl, 20 mmol/L cacodylate buffer maintained at *p*H 7.0 and 37 °C.

In order to demonstrate that the action of fluoride inhibition on lesion progression could be measured, a third model was used employing the same *p*H cycling regimen, however, 0.1 ppm fluoride was added to the remineralizing solution described above to inhibit lesion progression. The presence of fluoride accelerates remineralization and inhibits demineralization leading to slower lesion progression. A total of 15 sections were used with three sections for each time period.

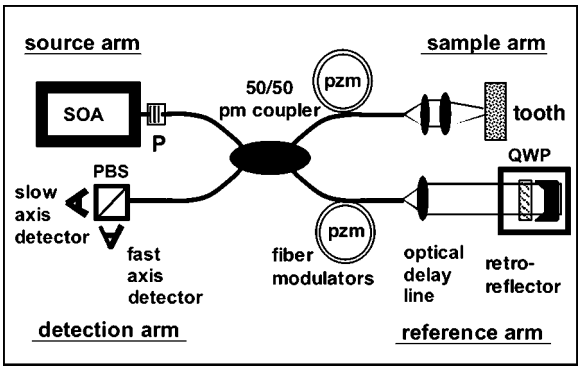

Fig. 1 PS-OCT system—light from the SOA broadband source is linearly polarized (P) and coupled into the slow axis of the polarization maintaining fiber of the source arm. Light from the source arm is equally split between the sample and reference arms of a fiber optic Michelson interferometer. The length of the reference arm can be manually adjusted using a linear stage to match the sample arm length. The path length difference between the sample and reference arms is varied using piezoelectric fiber stretchers (pzm). The maximum path length difference was varied by 6.8 mm at a rate of 10 Hz to produce a Doppler frequency shift of 200 kHz for heterodyne detection. A polarizing beam splitter (PBS) in the detection arm splits the fast (⊥) and slow (∥) axis components of the light onto the two detectors.

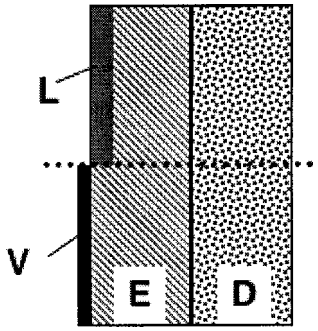

Fig. 2 A cross section of the tooth sections containing enamel (E) and dentin (D) used for artificial demineralization or simulated decay. Half the tooth enamel was covered with an acid resistant varnish (V) while the other half uncovered for exposure to demineralization to create the lesion (L).

2.2 Polarization Sensitive Optical Coherence Tomographic Imaging (PS-OCT)

An all fiber-based optical coherence domain reflectometry (OCDR) system that was designed and fabricated by Optiphase, Inc. (Van Nuys, CA) consisting of polarization maintaining (pm) optical fiber, high speed piezoelectric fiber stretchers and two balanced InGaAs receivers was used to acquire the images presented. This two-channel system was integrated with a broadband high power (26 mW) semiconductor optical amplifier (SOA), a BBS1310 from JDS Uniphase (Ottawa, Canada) and a high-speed XY-scanning system with a ESP 300 controller and 850G-HS stages from Newport (Irvine, CA) for *in vitro* optical tomography. A schematic of the system is shown in Figure 1.

Linearly polarized light was incident on the tooth samples and the backscattered intensity in both orthogonal polarizations was measured in each detector channel. The OCDR system is based on a polarization-sensitive Michelson white light interferometer. The high power (26 mW) SOA diode source operating at a center wavelength of 1310 nm with a spectral bandwidth full width at half maximum of 50 nm was passed through a linear polarizer, providing 13 mW of horizontally polarized light. This light was coupled into the slow axis of the polarization maintaining (pm) fiber of the source arm of the interferometer. This light was split into the reference and sample arms of the Michelson interferometer by a 50/50 pm-fiber coupler. The sample arm was coupled to an antireflection (AR) coated fiber collimator to produce a collimated beam with a diameter of 6 mm. That beam was focused onto the sample surface using a 20 mm focal length AR coated plano-convex lens to yield a minimum spot diameter of ($1/e^2$) of 33 μm. The spot size was determined by manually scanning a razor blade across the beam to acquire the spatial beam profile. The autocorrelation function was measured using a mirror yielding a depth resolution of 30 μm. Both orthogonal polarization states of the light scattered from the tissue were coupled into the slow and fast axes of the pm fiber of the sample arm. A quarter wave plate set at 22.5° to horizontal in the reference arm rotated the polarization of the light by 45° upon reflection. After being reflected from the retro reflector, the sample and reference beams were recombined by the pm fiber coupler. A polarizing cube splits the recombined beam into its horizontal and vertical polarization components or ''slow'' and ''fast'' axis components, which were then coupled by single mode fiber optics into each detector. The light from the reference arm was polarized at 45° and therefore split evenly between the two detectors. Readings of the electronically demodulated signal from each receiver channel represent the intensity for each orthogonal polarization of the backscattered light. Neutral density filters are added to the reference arm to reduce the intensity noise for shot limited detection. The PS-OCT system was completely controlled using Labview™ software from National Instruments (Austin, TX). The OCDR demodulator was operated with a Doppler frequency of 200 kHz. The piezoelectric fiber modulators (pzm), were used in a push–pull configuration for a total path difference $\sim$7 mm. Cross-sectional images or b scan files were acquired by moving the tooth samples every 10 μm at a rate of 10 scans/sec. Image processing was carried out using Igor Pro™, data analysis software from Wavemetrics Inc. (Lake Oswego, Oregon).

2.3 Optical and X-Ray Microscopy

Whole teeth with natural occlusal lesions were sectioned with a microtome and examined at up to 500× magnification under bright field and dark field illumination with an optical microscope (Olympus BX-50, Olympus America, Melville, NY) interfaced to a high-resolution digital camera DVC 1300C (DVC Company Inc, Austin, TX) with Image Pro Plus image analysis software (Media Cybernetics, Silver Spring, MD). Measurements of lesion depth were made with calibrated image analysis software that is capable of direct length and area measurements.

X-ray tomographic microscopy (XTM) was used to provide tomographic images of mineral density in lesion areas without the destruction of the tooth and these images were used for direct comparison with optical tomographic images acquired using PS-OCT. One of the advantages of XTM is that tissue slices representing the mineral density versus position can be extracted from the x-ray tomogram with any desired orientation to match the OCT scan geometry. OCT b scans were precisely matched with a corresponding tissue slice of mineral density taken from an x-ray tomogram. Complete tomographic images of tooth sections were acquired with a 9 μm spatial resolution, using the Stanford Linear Accelerator as described by Kinney et al.[42,43] A Sun microcomputer workstation and IDL software (Research Systems Inc., Boulder, CO) was used to exact slices of mineral density in the tooth matching the geometry of the OCT scans without the destruction of the tooth section.

3 Results

3.1 Initial Test Samples—Polished Sound Bovine Tooth Sections

Initial images were acquired by scanning across the surface of flat 5×5 mm^2 highly polished sections taken from bovine incisors $\sim$2 mm thick with an outer layer of enamel of $\sim$1 mm thickness. The incident light on the tooth leaving the pm fiber was linearly polarized with the electrical field aligned with the slow axis of the fiber. Three sections were imaged and PS-OCT 6-scans from one of the bovine samples are shown in Figure 3 for both orthogonal polarizations, each defined according to their respective alignment with the fast and slow axes of the pm fiber. The images are presented using a red-white-blue false color table and there was no post imaging smoothing or editing of the images. The axial scale is plotted as the optical depth, the product of physical depth and the refractive index of each medium. The slow axis image shows the intensity of light that is reflected/backscattered in the *original* polarization. At the surface there is a very strong signal due to the specular reflection from the enamel-air interface. This surface reflection is particularly strong for normal incidence and the intensity varies markedly with angle of incidence. The intensity in this region is 20 dB higher than the scattering intensity in other areas of the slow-axis image; therefore it masks any information about scattering at or just below the tooth surface. Moreover, the strong signal can lead to residual coherence artifacts (spikes) in the image (see image of Figure 6). The surface reflection appears weak in the

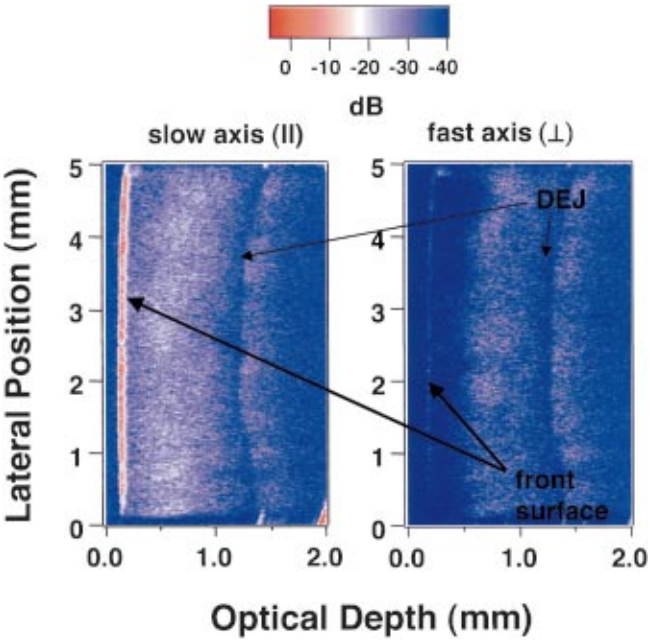

Fig. 3 Slow (||) (left) and fast (⊥) (right) axis images of a polished bovine enamel block with incident linearly polarized light aligned with the slow axis of the pm fiber. The polished surface is visible in the slow axis image, since the specular reflection from the surface does not depolarize the light. The DEJ is clearly visible in both images at an optical depth of ~1.4 mm.

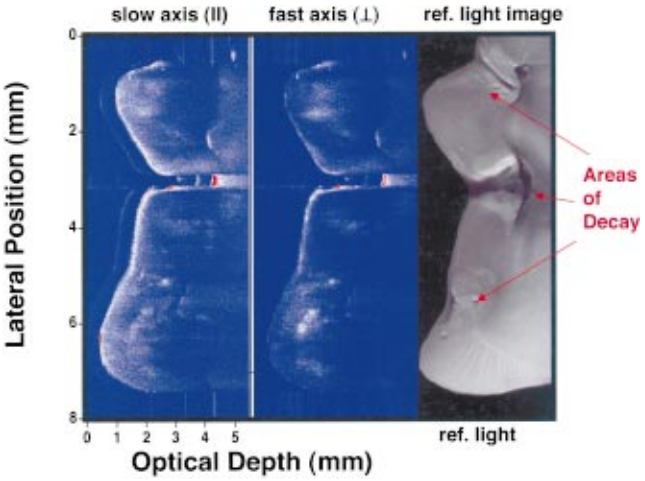

Fig. 5 Slow (||) and fast axis (⊥) OCT scans across the top of a third molar with occlusal decay. The reflected light image of the tooth section is shown on the right for comparison. All three carious areas are resolved in the OCT images with very strong scattering (red) in the base of the fissure shown in the center. The intensity varies from −40 to 10 dB with intensities of less than −39 dB demarcated in blue and those of intensity greater than 5 dB in red.

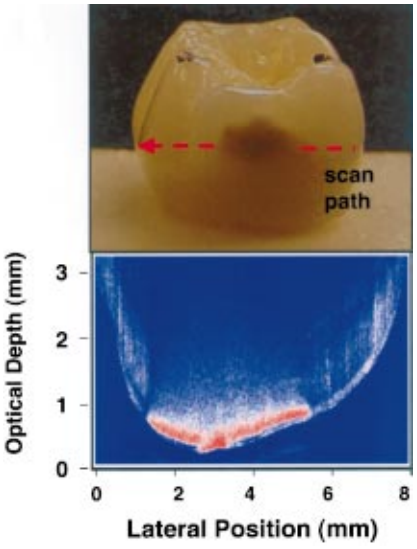

Fig. 4 Fast axis (⊥) OCT scan (bottom) of an obvious smooth surface inter-proximal lesion (white spot lesion). The path of the scan is shown in red in the reflected light image illuminated from the backside of the tooth (top). The dark areas on the tooth surface indicate the position of the lesion—the darker spot at the center is the small defect. The intensity in the false color image ranges from −37 dB (blue) to 5 dB (red).

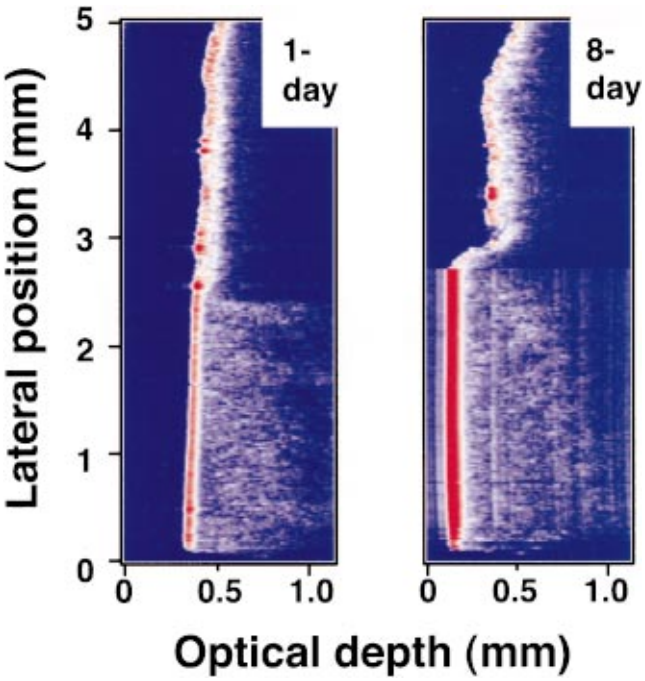

Fig. 6 Slow axis (||) OCT scans of artificially demineralized bovine enamel exposed to demineralization at *p*H 4.3 for one day (left) and eight days (right). The area above the dotted line was exposed to the demineralization solution while the area below the dotted line was protected with acid resistant varnish. Note the erosion of the surface over time. Although the amount of surface erosion can be quantified, the specular reflection masks the signal from the lesion area in the slow axis (||) images. Note the multiple reflections or coherence spikes that are produced by the very strong specular reflection at normal incidence from the surface (bottom right). These multiple reflections interfere with the signal from within the tooth.

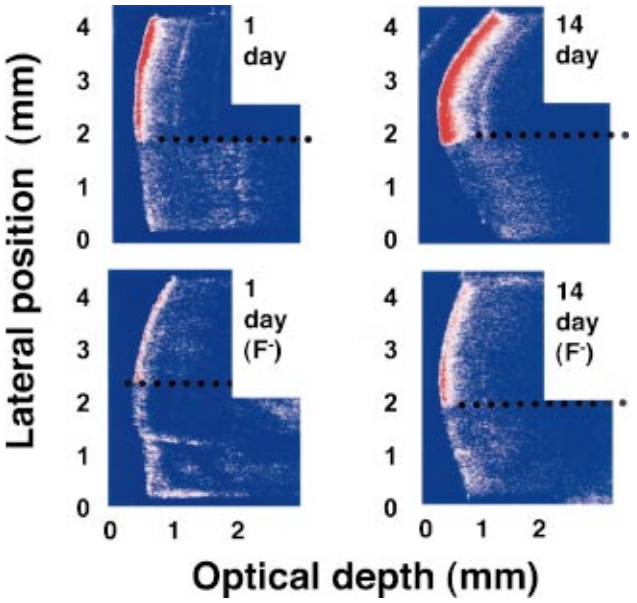

Fig. 7 PS-OCT scans of artificial enamel exposed to a simulated caries, *p*H cycling regimen for one and 14 days. The area above the dotted line is the treated area. Below the dotted line is the sound enamel—the untreated area that was covered by acid-resistant varnish. (Top) Human enamel exposed to *p*H cycling for one day (left) and 14 days (right). Fast-axis (⊥) images are shown since the confounding influence of the strong surface reflection is not present, allowing resolution of the demineralized areas near the surface. The reflected signal is greater after 14 days and has increased in severity and depth. (Bottom) Human enamel exposed to *p*H cycling for one day (left) and 14 days (right) with 0.1 ppm F^- added to the remineralization solution to inhibit decay. The lesion is smaller (30 μm deep) vs (120 μm) after 14 days due to fluoride incorporated into the remineralizing solution.

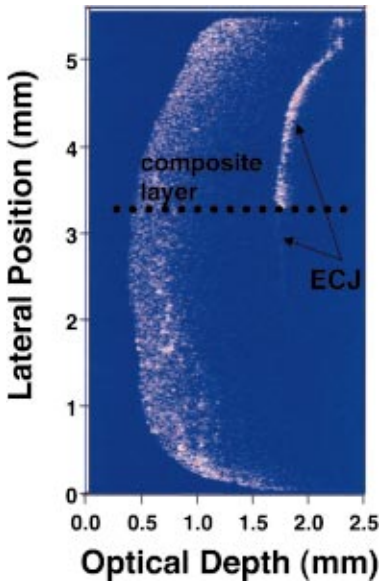

Fig. 9 Fast-axis (⊥) scans across one of the blocks of human enamel with one half demineralized (see Fig. 7) after 14 days *p*H cycling with the block covered with a layer of filled composite from 1 to 2 mm thickness. Demineralized enamel is visible below approximately 1–1.5 mm of composite at the enamel-composite junction (ECJ). Above the dotted line is demineralized enamel and below the dotted line is sound enamel. PS-OCT can resolve differences in mineralization below a thick layer of filled composite.

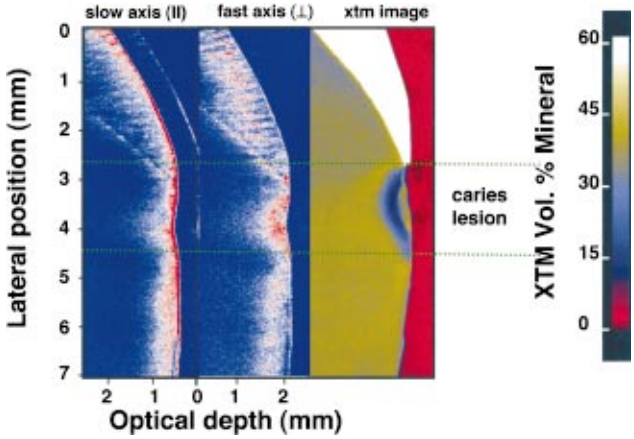

Fig. 10 Comparison of the slow (||) (left) and fast (⊥) (middle) axis images of a small section of a tooth with the x-ray tomogram (XTM) of the mineral density taken from the same region of the tooth (right). A small root caries lesion is present just below the cementum-enamel junction shown between the dotted green lines. The intensity of the OCT images ranges from 12 to −45 dB, areas with regions of intensity greater than −5 dB shown in red and those areas of less than −35 dB shown in blue. In the XTM image on the right, normal dentin is yellow, enamel is white, the water outside the tooth is indicated in red and the demineralized area of the lesion is blue (color bar for XTM Vol. % mineral to right).

fast axis image since the polarization of the incident light remains unchanged upon reflection and does not contribute intensity to the orthogonal polarization. At an optical depth of ~1.4 mm the dentin-enamel junction (DEJ) is clearly visible. This corresponds to the physical depth of the DEJ in the tooth section. The scattering coefficient of dentin is much higher than for the enamel and therefore the signal from the dentin appears stronger than the peripheral enamel, i.e., 10–20 dB stronger than the enamel signal that exponentially decreases to below −30 to −40 dB after penetrating to a depth of 1 mm.

3.2 Natural Interproximal Lesion—Smooth Surface "White Spot" Lesions

Interproximal lesions or smooth surface lesions were the first natural lesions to be investigated since the decay hidden between the teeth is readily visible once the tooth has been extracted. An optical image of such a lesion on an extracted human tooth is shown in Figure 4 under dark-field illumination. Under dark-field illumination the highly scattering areas of the lesion appear dark. A fast axis (⊥) b scan of lateral position versus depth taken across the center of the lesion along the path shown by the arrow in the optical image is shown in the same figure. Intense scattering and depolarization from the lesion area is shown—demarcated in red on the false color image. A surface zone is visible on part of the lesion, in addition to the full body of the lesion. This is the thin weakly scattering zone on the outside of the lesion to the left and the right of the central defect or darker spot that is barely visible in the reflected light image. These may be areas of the lesion that have remineralized. Surface remineralization leads to reduced scattering in the remineralized lesion areas due to filling of the micropores. The outer zone of the caries lesion is of particular importance for determination of the lesion activity. An outer zone of reduced scattering, indicative of remineralization, may be a potential indicator that the lesion is arrested and that intervention may not be necessary. Strong reflection from the surface in the slow-axis image (not shown) confounds measurement of the surface zone at the lesion surface.

3.3 Natural Occlusal Lesion

Since PS-OCT uses coherent backscattered and reflected light, as opposed to transmitted light, it is ideally suited for the detection of early occlusal lesions. Slow (∥) and fast axis (⊥) b scans acquired of an intact tooth with occlusal decay are shown in Figure 5. The reflected light, bright-field image acquired of a cross section of the tooth, after it was sectioned subsequent to acquisition of the OCT image, is shown in the right hand image of the same figure. Demineralized areas appear whiter due to increased scattering in the reflected light image. Those areas of decay are visible in the PS-OCT images, most significantly, the decay at the base of the central fissure (red area).

3.4 Longitudinal Studies of Simulated-Caries Lesions

Since the images of Figures 3–5 and our previous work described in Ref. 34 suggest that PS-OCT can provide information regarding lesion severity, we postulated that PS-OCT could be used to monitor lesion progression over time. To test this hypothesis, simulated caries lesions were monitored over time after exposure to various degrees of demineralization using three different simulated-caries models.

Straight Demineralization (Erosion) Model on Polished Bovine Sections (5×5×2 mm³)

The two slow-axis (∥) images of Figure 6 represent two samples exposed to a demineralizing solution after one day and eight days. The surface is gradually eroded over time leaving a cavitated zone. After eight days exposure to demineralization the depth of erosion is obviously greater than after one day. Note that in these slow axis images the strong specular refection from the surface obscures the scattering from the demineralized area of the lesion. This observation further demonstrates that the fast axis images are necessary to measure the enhanced scattering associated with the body of the lesion itself.

pH Cycling Models on Human Sections (4×4×2 mm³)

The fast-axis (⊥) images of Figure 7 show sample lesions produced using a *p*H cycling model after one day and 14 days. In the more realistic *p*H cycling model, an intact surface layer in the lesion is produced and erosion does not occur. The OCT images manifest a marked change in lesion severity with an increase in the depth and intensity of scattering from the lesion. In the *p*H cycling model the depth and severity of the lesion increases as the square root of the time.[41,44,45] In cross section under microscopic observation at 500 × magnification the lesion zone is not yet visible after one day of cycling; after 14 days it has progressed to a depth of 80–120 μm which is consistent with the optical depth of ~200 μm measured with OCT (see Figure 8). The set of images on the bottom of Figure 7 are scans of lesions produced after the addition of 0.1 ppm fluoride. The fluoride inhibits lesion progression over time and this is reflected in the OCT image of the lesion produced after 14 days. Lesion cross sections indicate that the lesion has progressed to a physical depth of only 20–30 μm after 14 days.

Depth profiles were extracted at single lateral positions from the fast-axis OCT scans from both demineralized and sound areas on each of the treated blocks, 25 with fluoride and 15 without. Depth profiles are shown in Figure 8 for one of the samples subjected to 14 days of cycling. Both the demineralized area above the dotted line of Figure 7 and below the dotted line in the sound enamel is shown. The depth profiles were integrated over the respective lesion areas, to a depth of 200 μm, and an equivalent area of the sound tissue on each tooth sample to yield the integrated intensity from the lesion area. The mean ± s.d. of the integrated scattering intensity is plotted from both the demineralized and sound areas of each sample for each set of five samples scanned for each cycling period vs. the square root of time in Figure 8. The Pearson correlation coefficient (r) derived from linear regression for the mean integrated scattering intensity from the lesion areas versus the square root of time of *p*H cycling is 0.96. There is no apparent correlation between the integrated scattering intensity with the square root of time, $r = -0.1$ for the sound (untreated) areas. The slope of the integrated scat-

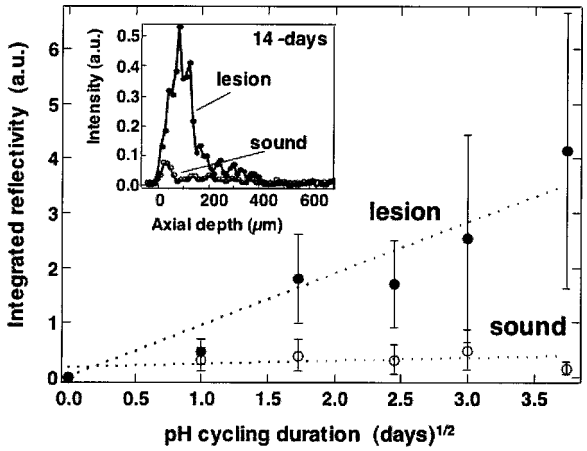

Fig. 8 The integrated reflected light intensity with depth extracted from the images acquired after *p*H cycling for 1, 3, 6, 9, and 14 days (see Fig. 7) plotted vs the square root of time. The solid symbols represent the integrated signal from the demineralized area of enamel—red area of Fig. 7 above the dotted line and the open symbols the sound area—below the dotted line. The dotted lines represent linear fits to the sound and demineralized areas, respectively. There are five samples per point with the mean ± s.d. represented in the plot. (Inset) Depth profiles of the reflected/scattered light intensity extracted from the fast axis image acquired after 14 days of *p*H cycling (see Fig. 7, top right). The solid symbols represent the demineralized area of enamel—red area of Fig. 7 above the dotted line and the open symbols the sound area—below the dotted line.

tering intensity from the demineralized lesion area was significantly different from zero ($P<0.001$, $n=25$, Student t test). Linear fits to the means are shown in Figure 8 as the dotted lines.

3.5 Simulated Lesion Beneath Dental Composite (Decay Underlying Restorations)

In order to determine if PS-OCT can be used effectively to determine the state of mineralization beneath a composite restoration, a thick layer of composite was added to the surface of one of the blocks used for the *p*H cycling studies described in the previous section. A layer of filled composite (Z100, 3M, St. Paul, MN) of approximately 1–1.5 mm thickness was applied to the surface of one human tooth section after exposure to 14 days of *p*H cycling according to the manufacturer's instruction. A fast-axis (⊥) image of the composite covered section is shown in Figure 9. Differences in the intensity of the reflected/scattered light from the sound and lesion areas are clearly apparent beneath the thick layer of composite. These images indicate that light can penetrate through the filled composite restorative material for monitoring secondary caries around existing composite restorations and pit and fissure sealants.

Other images were acquired of composite bonded adjacent to enamel and dentin. These images show that PS-OCT is useful for differentiating between composite and dental hard tissue. Typically the slow axis images show relevant interfaces, however the scattering is of a similar magnitude in both the normal enamel and from the body of restorative material. In contrast, the corresponding fast-axis image shows a marked difference in intensity between the scattering in the normal enamel and the composite. We suspect that the difference is due to the native birefringence of the enamel that contributes to signal in the fast-axis (⊥) channel. This difference is even more profound between dentin and composite. Therefore, the fast-axis images are useful for differentiating composite from dentin and enamel.

3.6 Natural Early Root Caries Lesion

It is difficult to obtain intact thin sections through natural root caries lesions without damage to the fragile, poorly mineralized regions of the lesion. Therefore, we used high-resolution x-ray tomography (XTM) to acquire tomograms of the mineral density in the tooth with a resolution of 9 μm.[42,43] A ''quartered'' tooth was scanned using the PS-OCT system from the crown to the root across a small root caries lesion located just below the cementum-enamel junction, Figure 10. Taking into account that the high refractive indices of dentin and enamel result in compression of those areas of the image, the agreement between the two imaging modalities is excellent. The entire lesion morphology is reproduced in the fast-axis OCT image with the characteristic lesion semicircle shape being clearly visible. The fast-axis image provides the best match since the confounding influence of the surface reflection and residual coherence are markedly reduced.

4 Discussion

These preliminary studies have demonstrated that PS-OCT has great potential for imaging early caries lesions and for monitoring lesion progression in enamel and dentin. In this study and in our previous study,[34] we have demonstrated that PS-OCT can be used to acquire high-resolution images of interproximal, occlusal and early root caries, and image through composite fillings or sealants. Depolarization due to scattering from anisotropic structures or phase retardation of the light (polarization rotation) induced by the native tissue birefringence lead to intensity in the orthogonal (⊥) polarization state or the fast-axis component. Polarization resolved images are invaluable for imaging changes in scattering at or near the enamel surface by removing the confounding influence of the intense reflectance at tissue interfaces. This is paramount for resolving very early caries lesions and for monitoring demineralization in simulated caries models. It is important to note that the use of circularly polarized light results in a strong surface reflection in each channel and is not as useful in this regard. As demonstrated previously, the PS-OCT images are also useful for differentiating the effects of native birefringence on the reflected (scattered) intensity.[34]

The dentinal-enamel junction (DEJ) at an optical depth of ~1.4 mm in sound enamel was resolved in both orthogonal polarizations. Scattering from the dentin below the DEJ is resolvable due to the markedly higher scattering of dentin, even though the backscattered light intensity from enamel falls below the noise floor before reaching the DEJ, at an optical depth of ~1.2 mm. Sound enamel weakly scatters near-IR light and produces a weak signal; this weak signal is further attenuated by scattering as the light penetrates through the tooth to an optical depth of 1.5 mm or physical depth in enamel of 1 mm with the current system. If a strong scatterer is present, such as demineralized enamel or dentin, then the decay can be differentiated at optical depths of 2–3 mm. Therefore, PS-OCT is capable of detecting demineralization

at the DEJ through the maximum possible thickness of enamel, 2–3 mm. After imaging several natural lesions with both a bulk optic system[34] and the all-fiber system, it is apparent that areas of subsurface demineralization and lesion structure can be imaged suitably with PS-OCT. Images of occlusal lesions show that PS-OCT provides useful depth resolved diagnostic information about the severity of occlusal lesions. These are the most important lesions for diagnosis due to both their prevalence and their hidden nature, since by the time they can be resolved on bitewing radiographs, it is much too late and they have penetrated well into the dentin.

Initial polarization resolved measurements by Baumgartner et al.[29] showed that PS-OCT can be used to measure birefringence in dental hard tissues. Later measurements by our group, Everett et al.,[34] demonstrated that caries lesions highly attenuate incident polarized light and lead to depolarization due to scattering. In this study we demonstrate for the first time that the intensity of linearly polarized light scattered into the perpendicular polarization state (depolarized) can be directly correlated with the degree of demineralization and lesion severity. Therefore, PS-OCT has enormous potential for monitoring changes in mineralization *in vivo* for short-term clinical studies of the efficacy of anti-caries agents. Since small diameter PS-OCT reflectance probes can be easily fabricated, this tool can potentially be used to monitor the effects of anti-caries agents in occlusal surfaces, in between teeth or beneath pit and fissure sealants. These are the sites at which 90% of dental decay occurs. Future measurements will seek to establish the relationship between the intensity of the PS-OCT images, the local mineral density in the lesion, and the integrated mineral loss across the lesion, i.e., the ΔZ value using microradiography.[45]

Acknowledgments

The work was supported by NIH/NIDCR Grants ROI-DE14698, P60-DE13058 and the UCSF Academic Senate. The investigators would also like to acknowledge Larry Watanabe at UCSF for his contributions and Jeff Bush and Steve Bell at Optiphase, Inc. for their help with the PS-OCT system.

References

1. J. D. B. Featherstone, ''Prevention and reversal of dental caries: role of low level fluoride,'' *Community Dent. Oral Epidemiol.* **27**, 31–40 (1999).
2. H. H. Chauncey, R. L. Glass, and J. E. Alman, ''Dental caries, principal cause of tooth extraction in a sample of U.S. male adults,'' *Caries Res.* **23**, 200–205 (1989).
3. L. M. Kaste, R. H. Selwitz, R. J. Oldakowski, J. A. Brunelle, D. M. Winn, and L. J. Brown, ''Coronal caries in the primary and permanent dentition of children and adolescents 1–17 years of age: United States, 1988–1991,'' *J. Dent. Res.* **75**, 631–641 (1996).
4. D. M. Winn, J. A. Brunelle, R. H. Selwitz, L. M. Kaste, R. J. Oldakowski, A. Kingman, and L. J. Brown, ''Coronal and root caries in the dentition of adults in the United States, 1988–1991,'' *J. Dent. Res.* **75**, 642–651 (1996).
5. B. Angmar-Mansson and J. J. ten Bosch, ''Optical methods for the detection and quantification of caries,'' *Adv. Dent. Res.* **1**(1), 14–20 (1987).
6. J. Vaarkamp, J. J. t. Bosch, and E. H. Verdonschot, ''Light propagation through teeth containing simulated caries lesions,'' *Phys. Med. Biol.* **40**, 1375–1387 (1995).
7. J. W. van de Rijke and J. J. ten Bosch, ''Optical quantification of caries-like lesions *in vitro*,'' *J. Dent. Res.* **69**(5), 1184–1187 (1990).
8. J. J. ten Bosch, H. C. van der Mei, and P. C. F. Borsboom, ''Optical monitor of *in vitro* caries,'' *Caries Res.* **18**, 540–547 (1984).
9. C. C. Ko, D. Tantbirojn, T. Wang, and W. H. Douglas, ''Optical scattering power for characterization of mineral loss,'' *J. Dent. Res.* **79**(8), 1584–1589 (2000).
10. D. Spitzer and J. J. ten Bosch, ''The absorption and scattering of light in bovine and human dental enamel,'' *Calcif. Tissue Res.* **17**, 129–137 (1975).
11. D. Fried, J. D. B. Featherstone, R. E. Glena, and W. Seka, ''The nature of light scattering in dental enamel and dentin at visible and near-IR wavelengths,'' *Appl. Opt.* **34**(7), 1278–1285 (1995).
12. R. J. Jones and D. Fried, ''Attenuation of 1310 and 1550 nm through dental enamel,'' *Lasers in Dentistry VII*, Vol. 4610, pp. 187–190, SPIE, San Jose, CA (2002).
13. A. Schneiderman, M. Elbaum, T. Schultz, S. Keem, M. Greenebaum, and J. Driller, ''Assessment of dental caries with digital imaging fiber-optic transillumination (DIFOTI): *In vitro* study,'' *Caries Res.* **31**, 103–110 (1997).
14. K. Koenig, H. Schneckenburger, J. Hemmer, B. J. Tromberg, R. W. Steiner, and W. Rudolf, ''*In-vivo* fluorescence detection and imaging of porphyrin-producing bacteria in the human skin and in the oral cavity for diagnosis of acne vulgaris, caries, and squamous cell carcinoma,'' *Advances in Laser and Light Spectroscopy to Diagnose Cancer and Other Diseases*, R. R. Alfano, Ed., Vol. 2135, pp. 129–138, SPIE, San Jose, CA (1994).
15. X. Q. Shi, U. Welander, and B. Angmar-Mansson, ''Occlusal caries detection with Kavo DIAGNOdent and radiography: An *in vitro* comparison,'' *Caries Res.* **34**, 151–158 (2000).
16. R. Hibst and R. R. Paulus, ''New approach on fluorescence spectroscopy for caries detection,'' *Bios 99*, R. Featherstone and D. Fried, Eds., Vol. 3593, SPIE, San Jose, CA (1999).
17. A. Lussi, S. Imwinkelreid, N. B. Pitts, C. Longbottom, and E. Reich, ''Performance and reproducibility of a laser fluorescence system for detection of occlusal caries *in vitro*,'' *Caries Res.* **33**, 261–266 (1999).
18. U. Hafstroem-Bjoerkman, F. Sundstroem, E. d. J. de Jong, A. Oliveby, and B. Angmar-Mansson, ''Comparison of laser fluorescence and longitudinal microradiography for quantitative assessment of *in vitro* enamel caries,'' *Caries Res.* **26**, 241–247 (1992).
19. H. Eggertsson, M. Analoui, M. H. v. d. Veen, C. Gonzalez-Cabezas, G. J. Eckert, and G. K. Stookey, ''Detection of early interproximal caries *in vitro* using laser fluorescence, dye-enhanced laser fluorescence and direct visual examination,'' *Caries Res.* **33**, 227–233 (1999).
20. U. Hafstrom-Bjorkman, F. E. de Josselin de Jong, A. Oliveby, and B. Angmar-Mansson, ''Comparison of laser fluorescence and longitudinal microradiography for quantitative assessment of *in vitro* enamel caries,'' *Caries Res.* **26**, 241–247 (1992).
21. M. D. Lagerweij, M. H. v. d. Veen, M. Ando, and L. Lukantsova, ''The validity and repeatability of three light-induced fluorescence systems: An *in vitro* study,'' *Caries Res.* **33**, 220–226 (1999).
22. J. A. Izatt, M. R. Hee, D. Huang, J. G. Fujimoto, E. A. Swanson, C. P. Lin, J. S. Schuman, and C. A. Puliafito, ''Optical coherence tomography for medical applications,'' in *Medical Optical Tomography: Functional Imaging and Monitoring*, G. Muller, B. Chance, R. Alfano, S. Arridge, J. Beuthan, E. Gratton, M. Kaschke, B. Masters, S. Svanberg, and P. v. d. Zee, Eds., Vol. IS11, pp. 450–472, SPIE, Bellingham, WA (1993).
23. D. Derickson, *Fiber Optic Test and Measurement*, Hewlett-Packard Professional Books, Prentice–Hall, Upper Saddle River, NJ (1998).
24. R. C. Youngquist, S. Carr, and D. E. N. Davies, ''Optical coherence-domain reflectometry,'' *Appl. Opt.* **12**, 158–160 (1987).
25. D. Huang, E. A. Swanson, C. P. Lin, J. S. Schuman, W. G. Stinson, W. Chang, M. R. Hee, T. Flotte, K. Gregory, C. A. Puliafito, and J. G. Fujimoto, ''Optical coherence tomography,'' *Science* **254**, 1178–1181 (1991).
26. B. Colston, M. Everett, L. Da Silva, L. Otis, P. Stroeve, and H. Nathel, ''Imaging of hard and soft tissue structure in the oral cavity by optical coherence tomography,'' *Appl. Opt.* **37**(19), 3582–3585 (1998).
27. B. W. Colston, M. J. Everett, L. B. Da Silva, H. Nathel, and L. L. Otis, ''Optical coherence tomography for diagnosis of periodontal diseases,'' *Laser in Dentistry III*, Vol. 2973, pp. 216–220, SPIE, San Jose, CA (1997).
28. B. W. Colston, U. S. Sathyam, L. B. DaSilva, M. J. Everett, and P. Stroeve, ''Dental OCT,'' *Opt. Express* **3**(3), 230–238 (1998).
29. A. Baumgartner, C. K. Hitzenberger, S. Dicht, H. Sattmann, A. Moritz, W. Sperr, and A. F. Fercher, ''Optical coherence tomography

for dental structures,'' *Laser in Dentistry IV,* Vol. 3248, pp. 130–136, SPIE, San Jose, CA (1998).
30. A. Baumgartner, S. Dicht, C. K. Hitzenberger, H. Sattmann, B. Robi, A. Moritz, W. Sperr, and A. F. Fercher, ''Polarization-sensitive optical optical coherence tomography of dental structures,'' *Lasers in Dentistry V,* Vol. 3593, pp. 169–176, SPIE, San Jose, CA (1999).
31. A. Baumgartner, S. Dicht, C. K. Hitzenberger, H. Sattmann, B. Robi, A. Moritz, W. Sperr, and A. F. Fercher, ''Polarization-sensitive optical optical coherence tomography of dental structures,'' *Caries Res.* **34**, 59–69 (2000).
32. F. I. Feldchtein, G. V. Gelikonov, V. M. Gelikonov, R. R. Iksanov, R. V. Kuranov, A. M. Sergeev, N. D. Gladkova, M. N. Ourutina, J. A. Warren, and D. H. Reitze, ''*In vivo* OCT imaging of hard and soft tissue of the oral cavity,'' *Opt. Express* **3**(3), 239–251 (1998).
33. X. J. Wang, J. Y. Zhang, T. E. Milner, J. F. d. Boer, Y. Zhang, D. H. Pashley, and J. S. Nelson, ''Characterization of dentin and enamel by use of optical coherence tomography,'' *Appl. Opt.* **38**(10), 2092–2096 (1999).
34. M. J. Everett, B. W. Colston, U. S. Sathyam, L. B. D. Silva, D. Fried, and J. D. B. Featherstone, ''Non-invasive diagnosis of early caries with polarization sensitive optical coherence tomography (PS-OCT),'' *Lasers in Dentistry V,* Vol. 3593, pp. 177–183, SPIE, San Jose, CA (1999).
35. L. L. Otis, B. W. Colston, M. J. Everett, and H. Nathel, ''Dental optical coherence tomography: A comparison of two *in vitro* systems,'' *Dentomaxillofac Radiol.* **29**(2), 85–89 (2000).
36. E. A. M. Kidd, ''Secondary caries,'' *Int. Dent. J.* **42**, 127–138 (1992).
37. NIH, ''Diagnosis and management of dental caries throughout life,'' NIH Consensus Statement 18 (2001).
38. J. J. ten Bosch and J. R. Zijp, ''Optical properties of dentin,'' in *Dentine and Dentine Research in the Oral Cavity,* S. A. L. a. V. Q. A. Thylstrup, Ed., pp. 59–65, IRL, Oxford, England (1987).
39. D. J. White, ''Use of synthetic polymer gels for artificial carious lesion preparation,'' *Caries Res.* **21**, 228–242 (1987).
40. D. J. White and J. D. B. Featherstone, ''A longitudinal microhardness analysis of fluoride dentifrice effects on lesion progression *in vitro*,'' *Caries Res.* **21**, 502–512 (1987).
41. J. D. B. Featherstone, M. M. O'Reilly, M. Shariati, and S. Brugler, ''Enhancement of remineralization *in vitro* and *in vivo*,'' in *Factors Relating to Demineralization and Remlneralization of the Teeth,* S. A. Leach, Ed., IRL, Oxford, UK (1986).
42. J. H. Kinney, D. L. Haupt, M. C. Nichols, T. M. Breunig, G. W. Marshall, and S. J. Marshall, ''The x-ray tomographic microscope: three dimensional perspectives of evolving structures,'' *Nucl. Instrum. Methods Phys. Res. A* **347**, 480–486 (1994).
43. J. H. Kinney, M. Balooch, D. L. Haupt, S. J. Marshall, and G. W. Marshall, ''Mineral distribution and dimensional changes in human dentin during demineralization,'' *J. Dent. Res.* **74**(5), 1179–1184 (1995).
44. J. D. B. Featherstone, R. Glena, M. Shariati, and C. P. Shields, ''Dependence of *in vitro* demineralization and remineralization of dental enamel on fluoride concentration,'' *J. Dent. Res.* **69**, 620–625 (1990).
45. J. D. B. Featherstone, J. M. ten Cate, M. Shariati, and J. Arends, ''Comparison of artificial caries-like lesions by quantitative microradiography and microhardness profiles,'' *Caries Res.* **17**, 385–391 (1983).